Aberration and second-harmonic imaging

Trond Varslot
Dept. of Mathematical Sciences
NTNU
Trondheim, Norway
Email: varslot@math.ntnu.no

Svein-Erik Måsøy
Dept. Circulation and Medical Imaging
NTNU
Trondheim, Norway
Email: svein-erik.masoy@ntnu.no

Bjørn A Angelsen
Dept. Circulation and Medical Imaging
NTNU
Trondheim, Norway
Email: bjorn.angelsen@ntnu.no

***Abstract*— Simulations are presented which indicate that imaging at the second-harmonic frequency does not solve the problem of ultrasonic wave aberration. The nonlinearity of acoustic wave propagation in biological tissue is routinely exploited in medical imaging, since the larger signal-to-noise ratio leads to better image quality in many applications. The major sources of noise in ultrasound images are aberration and multiple reflections between the transducer and tissue structures (reverberations), both of which are the result of large spatial variations in the acoustic properties of the tissue. These variations mainly occur close to the body surface, *i.e.* the body wall. As a result, the nonlinearly-generated second-harmonic is believed to alleviate both reverberations and aberrations. However, in the case of aberration, the second-harmonic is generated by an aberrated pulse. Thus, the second-harmonic will experience considerable aberration even if it is generated at a greater depth. Propagation of the acoustic backscatter through the body wall will expose the pulse to further aberration, equivalent to that of linear fundamental imaging.**

I. Introduction

In this paper, a simulation study of three-dimensional (3D) forward nonlinear propagation of ultrasonic fields in heterogeneous media is presented. The goal is to clarify the issue of second-harmonic imaging and ultrasonic wave aberration.

Harmonic imaging (HI), also known as tissue harmonic imaging or second-harmonic imaging, is today a standard choice of imaging modality in many medical ultrasound applications. Christopher has performed a comprehensive study of second-harmonic generation in homogeneous and heterogeneous tissue [1], [2]. He showed that the lateral resolution of the second-harmonic beam profile was slightly narrower than the same-frequency fundamental for a heterogeneous medium in all the investigated cases. He furthermore showed that the sidelobe level was substantially lower. This result is confirmed by Shen and Li [3].

In medical applications, reported improvements from the use of HI are typically improved range penetration, contrast resolution, lateral resolution, and reduced acoustic noise [4], [5], [6], [7], [8].

However, there is still some debate as to why harmonic imaging yields better images [9]. The amplitude for any reflected signal is much lower than that of the forward-propagating transmit-field. As a result the amount of second-harmonic generated by reflected signals is relatively much lower than that generated by the forward-propagating transmit-field; reverberations are substantially reduced in the second-harmonic. Other effects such as suppression of grating-lobes, lower side-lobes and reduced aberration because the second-harmonic is generated behind the aberrating body wall are also mentioned.

This paper is organised as follows. Section II desctibes the theoretical foundations for understanding aberration of the second-harmonic component. In Section III and IV the methods and results are presented, and in Section V conclusions are drawn.

II. Theory

There are many nonlinear wave equations available which aim at modeling acoustic wave propagation. One such equation is the generalised Westervelt equation which describes nonlinear wave propagation in a heterogeneous medium such as soft biological tissue (muscle, fat, blood, *etc.*). Under the assumption of constant mass density, it may be expressed in nondimensional form as

$$\nabla^2 p - \frac{1}{c^2}\frac{\partial^2 p}{\partial t^2} = -\epsilon_n \frac{\partial^2 p^2}{\partial t^2} + \frac{1}{c^2}\frac{\partial^2 \mathcal{L} p}{\partial t^2}. \tag{1}$$

Here p is the acoustic pressure, c is the speed of sound and ϵ_n is a nondimensional parameter [10]. To simplify notation, define the linear scattering operator q to be

$$q(r) = \frac{1}{c_0^2}\left(\frac{c_0^2}{c^2} - 1 + \frac{c_0^2}{c^2}\mathcal{L}\right). \tag{2}$$

Thus the wave equation may be written as

$$\nabla^2 p - \frac{1}{c_0^2}\frac{\partial^2 p}{\partial t^2} = q\frac{\partial^2 p}{\partial t^2} - \epsilon_n \frac{\partial^2 p^2}{\partial t^2}, \tag{3}$$

or equivalently in the temporal frequency domain

$$\nabla^2 \hat{p} + \frac{\omega^2}{c_0^2}\hat{p} = Q\omega^2 \hat{p} - \epsilon_n \omega^2 \hat{p} \underset{\omega}{*} \hat{p}. \tag{4}$$

In the latter equation $*_\omega$ indicates convolution with respect to frequency.

It is now instructive to define a *linear part* and a *nonlinear part* of the acoustic pressure, denoted p_l and p_{nl}, respectively. They are defined to satisfy the following equations

$$p = p_l + p_{nl} \tag{5}$$

$$\nabla^2 \hat{p}_l + \frac{\omega^2}{c_0^2}\hat{p}_l = Q\omega^2 \hat{p}_l \tag{6}$$

$$\nabla^2 \hat{p}_{nl} + \frac{\omega^2}{c_0^2}\hat{p}_{nl} = Q\omega^2 \hat{p}_{nl} + \epsilon_n \omega^2 \hat{p} \underset{\omega}{*} \hat{p}. \tag{7}$$

Aberration of the linear part has been studied by many authors. A list of some relevant references is found in Måsøy *et al.* [11]. It has been shown that a good description of the aberration is supplied by the generalised frequency-dependent screen, or its approximation by a time-shift and amplitude screen. In this case the pressure at a point r is calculated as [12]

$$\hat{p}_l(r) = \int_T g(r-\xi)s(r,\xi)\hat{p}_0(\xi)\mathrm{d}\xi, \tag{8}$$

where g is the appropriate Green's function, p_0 is the wave form transmitted from the transducer array, and integration is performed over the transducer surface T.

If $|p_{nl}| << |p_l|$, then a linearisation is reasonable

$$p = p_l + p_{nl} \tag{9}$$

$$\nabla^2\hat{p}_l + \frac{\omega^2}{c_0^2}\hat{p}_l = Q\omega^2\hat{p}_l \tag{10}$$

$$\nabla^2\hat{p}_{nl} + \frac{\omega^2}{c_0^2}\hat{p}_{nl} = Q\omega^2\hat{p}_{nl} + \epsilon_n\omega^2\hat{p}_l \underset{\omega}{*} \hat{p}_l. \tag{11}$$

If p_l is a narrow-band pulse centered around the frequency ω_0 (the fundamental frequency), then p_{nl} will be a narrow-band pulse centered around $2\omega_0$; the second-harmonic frequency. The aberrated linear part is therefore a source of the nonlinear part. The nonlinear part is then aberrated further as it propagates through the tissue.

Therefore, in terms of time-delay the nonlinear part experiences the same aberration as the linear part. Furthermore, the ability to smooth out amplitude variations will decrease as a function of increased frequency. It is therefore reasonable to expect the aberration amplitude to be more severe for higher frequencies. As a consequence, the aberration of the second-harmonic part of the transmit-beam should be as aberrated as the fundamental.

In order to evaluate where the nonlinear part is generated the following quantity was used

$$E(z) = \int_{T_z}\int_{-\infty}^{\infty} |p(r)|^2 \mathrm{d}t\mathrm{d}\xi_z. \tag{12}$$

This is proportional to the total acoustic energy of the field in the plane T_z at depth z, and is therefore denoted the *total acoustic energy at depth* z in this paper. The slope of this function is a measure of the amount of energy generated at that depth.

III. Method

A 3D numerical experiment was conducted using a simulation setup capable of capturing nonlinear propagation and absorption in heterogeneous tissue [10]. An ultrasound pulse of 2.5 MHz, using an aperture of 2.0×2.0 cm, focused at 6.0 cm, was propagated through a body wall model of thickness 2.0 cm with aberration characteristics comparable to published measurements of the human abdominal wall. The body wall was constructed using procedures presented by Måsøy *et al.*[13].

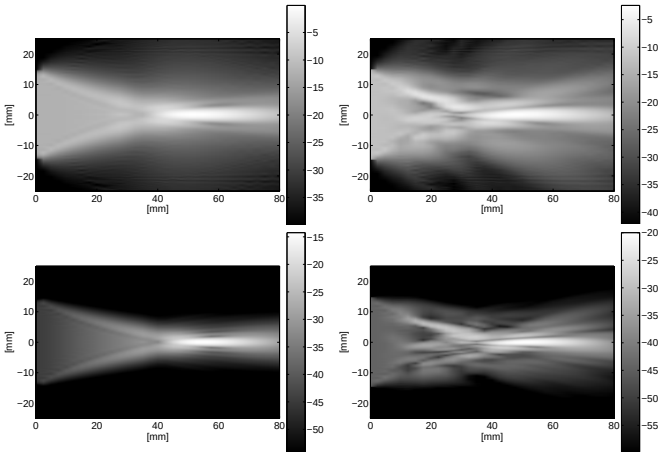

Fig. 1. Acoustic energy distribution in the xz-plane. The left column shows the unaberrated case, and the right column shows the aberrated case. Top: Energy in fundamental frequency band of 2.5 MHz. Bottom: Energy in the second-harmonic frequency band of 5 MHz.

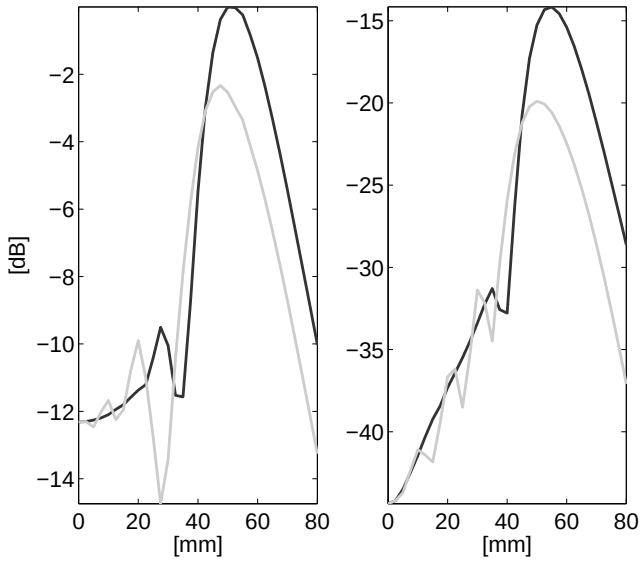

Fig. 2. Pressure amplitude along the transducer centre axis. Left: Amplitudes of the fundamental compared for unaberrated case (black) and aberrated case (gray). Right: Amplitude for the second-harmonic compared for unaberrated case (black) and aberrated case (gray).

IV. Results

Figure 1 shows the acoustic energy distribution in a plane through the beam axis, perpendicular to the transducer surface; the xz-plane. Aberration is clearly visible for both the linear part and the second-harmonic part of the field.

The peak pressure amplitude along the transducer centre axis is plotted in Fig. 2. It is seen that aberration reduces the amplitude by 2 dB for the fundamental, while a 6 dB reduction is observed for the second-harmonic.

In Fig. 3 the total acoustic energy as a function of depth is plotted (see Eq. (12)). The total energy of the fundamental decreases almost linearly both for the aberrated and the un-

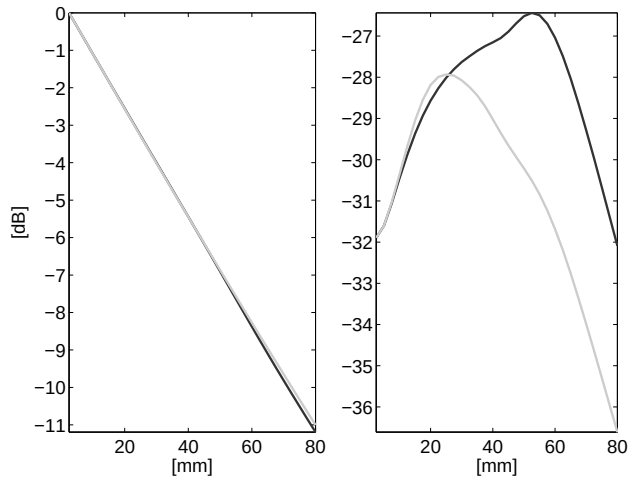

Fig. 3. Total energy as a function of depth. Left: Energy of the fundamental compared for unaberrated (black) and the aberrated (gray) simulation. Right: Energy of the second-harmonic compared for unaberrated case (black) and aberrated case (gray).

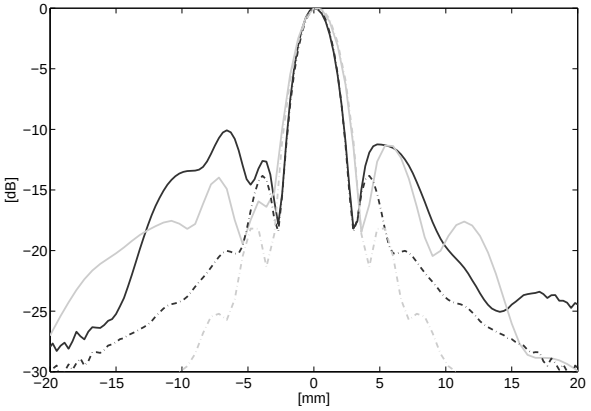

Fig. 4. Beam profiles in the focal plane of the transducer array. Axis for the second-harmonic is scaled to compare profile shapes. Aberrated profiles for the fundamental (solid black) and the second-harmonic (solid gray), and unaberrated profiles for the fundamental (dash-dot black) and the unaberrated second-harmonic (dash-dot gray).

aberrated simulations. The second-harmonic energy increases steadily towards the peak pressure of the fundamental in the unaberrated case (see Fig.2). For the aberrated case the energy peaks at about 2.5 cm, well before the peak pressure location and just after the body wall model.

Figures 4-5 show the beam profiles for the fundamental and second-harmonic in the focal plane. The axis has been reduced by a factor of 2 for the second-harmonic in order to compare the shape of the profiles. The aberrated profiles show clear similarities, with some differences in sidelobe levels.

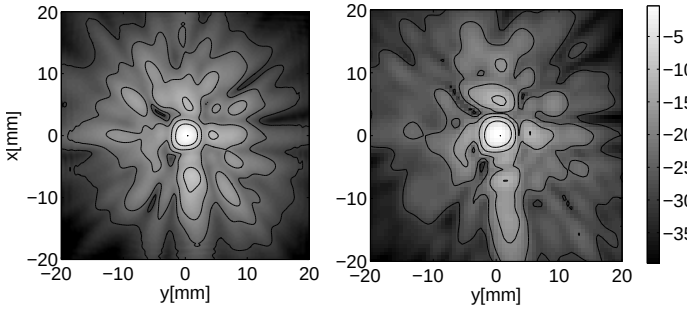

Fig. 5. Beam profiles in the focal plane of the transducer array. Axis for the second-harmonic is scaled to compare profile shapes. Left: Aberrated fundamental profile. Right: Aberrated second-harmonic profile.

V. Conclusion

For the unaberrated situation, the results show that close to the transducer there is almost a constant growth of the total energy for the second-harmonic. Approaching the focal region the focusing is weaker, and the growth is reduced. The point of maximum energy coincides with the maximum peak pressure along the transducer axis.

Aberration introduces a defocusing of the beam, and the growth in total energy for the second-harmonic peaks at approximately 2.5 cm. Beyond this point, the aberration of the beam is sufficiently strong for the absorption to dominate the production of second-harmonic energy. Still, there is an increase in the peak pressure of the second-harmonic along the transducer axis, mainly caused by focusing of the already generated second-harmonic field. The peak pressure curves along the transducer axis does not correctly indicate where the second-harmonic energy is generated in this case.

The results show that most of the second-harmonic generation occurs prior to the focal zone (extreme near-field) for the unaberrated case. The beam volume reduction and pressure increase due to focusing ensures a constant production of the second-harmonic in the extreme near-field. The focusing pressure increase halts in the focal zone, and absorption becomes dominating. When aberration is present, a similar situation is observed. However, the peak pressure reaches a lower value in this situation. Therefore, the reduced beam volume is not sufficiently compensated by the pressure increase due to focusing and the absorption dominates at an earlier stage.

As a result of the reduced focusing of the fundamental due to aberration, less second-harmonic energy is generated. In the presented simulations a reduction of 2 dB in peak pressure value for the fundamental implied a 6 dB reduction in peak pressure values for the second-harmonic. Harmonic imaging will therefore be more susceptible to general signal-to-noise

reduction due to aberration than fundamental imaging.

The shapes of the aberrated fundamental and second-harmonic show clear similarities. This may be understood by using the quasi-linear approximation, in which the fundamental acts as the generating source for the second-harmonic. When using second-harmonic imaging in modern ultrasound scanners, the fundamental frequency is reduced compared to standard fundamental imaging. The reduced frequency leads to a reduction in the aberration of the fundamental beam due to the increase in wavelength [14, pp. 11.31]. The aberration of the second-harmonic mimics that of the fundamental, and is therefore also reduced as a consequence of this wavelength increase.

In an imaging situation the acoustic backscatter which is received at the transducer array is subject to the same aberration as the transmitted wave. However, due to the much lower amplitude of the backscatter, there is no generating source term to stabilise the second-harmonic on the way back. Second-harmonic imaging does therefore not have an effect on the aberration of the received backscatter.

The presented results indicate that harmonic imaging may have limited effect on aberration. The observed signal-to-noise improvement using second-harmonic imaging are therefore most likely caused by the other factors such as reduced reverberation.

ACKNOWLEDGEMENT

This work was financed by the Norwegian University of Science and Technology.

REFERENCES

[1] T. Christopher, "Finite amplitude distortion-based inhomogeneous pulse echo ultrasonic imaging," *IEEE Trans. Ultrason. Ferroelectr. Freq. Control*, vol. 44, no. 1, pp. 125–139, 1997.

[2] ——, "Experimental investigation of finite amplitude distortion-based, second harmonic pulse echo ultrasonic imaging," *IEEE Trans. Ultrason. Ferroelectr. Freq. Control*, vol. 45, no. 1, pp. 158–162, 1998.

[3] C.-C. Shen and P.-C. Li, "Harmonic leakage and image quality degradation in tissue harmonic imaging," *IEEE Trans. Ultrason. Ferroelectr. Freq. Control*, vol. 48, no. 3, pp. 728–736, 2001.

[4] T. S. Desser, R. B. Jeggrey, M. J. Lane, and P. W. Ralls, "Tissue harmonic imaging: Utility in abdominal and pelvic sonography," *J. Clinic. Ultras.*, vol. 27, no. 3, pp. 135–142, March/April 1999.

[5] F. Tranquart, N. Grenier, V. Eder, and L. Pourcelot, "Clinical use of ultrasound tissue harmonic imaging," *Ultras. in Med. and Biol.*, vol. 25, no. 6, pp. 889–894, 1999.

[6] M. A. Averkiou, "Tissue harmonic ultrasonic imaging," *Opt. and Acous. Imag. of Biol. Media*, pp. 1139–1151, 2001.

[7] S. J. Rosenthal, P. H. Jones, and L. H. Wetzel, "Phase inversion tissue harmonic sonographic imaging: A clinical utility study," *AJR*, vol. 176, pp. 1393–1398, 2001.

[8] T. Hosono, Y. Chiba, H. Kanai, and T. Kanagawa, "Initital experiences of tissue harmonic imaging in the diagnosis of fetal cardiac tumors," *Ultras. in Obstet. and Gynecol.*, vol. 19, pp. 400–402, 2002.

[9] F. Duck, "Nonlinear acoustics in diagnostic ultrasound," *Ultrasound in Med. and Biol.*, vol. 28, no. 1, pp. 1–18, 2002.

[10] T. Varslot and G. Taraldsen, "Computer simulation of forward wave propagation in soft tissue," *IEEE Trans. Ultrason. Ferroelectr. Freq. Control*, vol. 52, no. 9, pp. 1473–1782, 2005.

[11] S.-E. M˚asøy, T. Varslot, and B. Angelsen, "Iteration of transmit-beam aberration correction in medical ultrasound imaging," *J. Acoust. Soc. Am.*, vol. 117, no. 1, pp. 450–461, 2005.

[12] ——, "Estimation of ultrasonic wave aberration with signals from random scatterers," *J. Acoust. Soc. Am.*, vol. 115, no. 6, pp. 2998–3009, June 2004.

[13] S. E. M˚asøy, T. F. Johansen, and B. Angelsen, "Correction of ultrasonic wave aberration with a time delay and amplitude filter," *J. Acoust. Soc. Am.*, vol. 113, no. 4, pp. 2009–2020, April 2003.

[14] B. A. Angelsen, *Ultrasound imaging. Waves, signals and signal processing*. Trondheim, Norway: Emantec, 2000, vol. 2, http://www.ultrasoundbook.com.